

## Fundamental Dynamics of Popularity-Similarity Trajectories in Real Networks

Evangelos S. Papaefthymiou, Costas Iordanou<sup>✉</sup>, and Fragkiskos Papadopoulos<sup>✉\*</sup>

*Department of Electrical Engineering, Computer Engineering and Informatics,  
Cyprus University of Technology, 3036 Limassol, Cyprus*

 (Received 25 September 2023; revised 27 November 2023; accepted 15 April 2024; published 17 June 2024)

Real networks are complex dynamical systems, evolving over time with the addition and deletion of nodes and links. Currently, there exists no principled mathematical theory for their dynamics—a grand-challenge open problem. Here, we show that the popularity and similarity trajectories of nodes in hyperbolic embeddings of different real networks manifest universal self-similar properties with typical Hurst exponents  $H \ll 0.5$ . This means that the trajectories are predictable, displaying antipersistent or “mean-reverting” behavior, and they can be adequately captured by a fractional Brownian motion process. The observed behavior can be qualitatively reproduced in synthetic networks that possess a latent geometric space, but not in networks that lack such space, suggesting that the observed subdiffusive dynamics are inherently linked to the hidden geometry of real networks. These results set the foundations for rigorous mathematical machinery for describing and predicting real network dynamics.

DOI: [10.1103/PhysRevLett.132.257401](https://doi.org/10.1103/PhysRevLett.132.257401)

Modeling and prediction of network dynamics, i.e., of the connections and disconnections that take place in a given network over different timescales, is perhaps the most fundamental unresolved problem in complex networks [1], listed also in the popular 23 Mathematical Challenges of DARPA [2]. Accurate prediction of such dynamics can unlock a plethora of applications across diverse domains, ranging from early detection and prevention of critical events in networked systems, to decision and policy making in financial markets, to strategic interventions for counterterrorism and public health [3,4].

We observe that the mathematical machinery and equations that describe the evolution of other complex dynamical systems and temporal data, such as gravitational and molecular systems, turbulence, and financial data, have been well developed and known for decades [5–9]. Yet, the underlying processes governing network dynamics and their mathematics remain elusive. One of the main reasons for this discrepancy is the fact that networks are discrete topological structures, not inheriting the standard form of temporal data met in other classical dynamical systems.

Advancements in network geometry during the past years revealed that real networks can be meaningfully mapped into continuous hyperbolic spaces [10–14]. In these spaces, nodes have radial (popularity) and angular (similarity) coordinates  $r$ ,  $\theta$ , and are connected in the observed network with a probability that decreases with their hyperbolic distance, determined by their coordinates [10]. Therefore, if the mathematics describing the evolution of the nodes' coordinates was known—and importantly, if this evolution were predictable—one could employ this mathematics to describe and ultimately predict connectivity dynamics. In essence, we observe that network geometry

provides a way to cast the problem of network dynamics to a time series prediction problem—a well-mined problem in other areas, such as finance [8,9,15,16], network traffic modeling [17,18], and fluid dynamics [19,20].

Given these considerations, here we analyze, for the first time, historical popularity and similarity trajectories of nodes in hyperbolic embeddings of different real networks and find that both types of trajectories exhibit subdiffusive dynamics (see Table I for the considered data). Specifically, we find that the trajectories are antipersistent with short-term negative autocorrelations, and can be well described by a fractional Brownian motion process [9].

In hindsight, these findings, and particularly the departure from the traditional law of Brownian motion, agree with intuition. Indeed, real networks are characterized by strong community structures and hierarchical organization that persist over time [45]. The first characteristic implies that similarity trajectories should remain confined within specific regions of the similarity space. The second characteristic signifies that popularity trajectories should fluctuate around some expected values that reflect the node positions in the network hierarchy or popularity space. For instance, a nonhub in the US air transportation network is expected to remain a nonhub even though its degree can fluctuate. Further, since the popularity and similarity trajectories are not generally independent, the dynamics of one can influence the dynamics of the other. This picture is analogous to subdiffusive phenomena found in crowded biological systems, where particles diffuse in environments with hierarchies of energy barriers or traps [46].

These findings have both practical and theoretical implications. From a practical perspective, the subdiffusivity of the trajectories implies that they are predictable

TABLE I. Overview of the considered networks, obtained from Refs. [21–25] (see Ref. [26], Sec. I, for details).

| Name          | Nodes              | No. of snapshots          |
|---------------|--------------------|---------------------------|
| US air        | US airports        | 10 000 (daily, 1988–2015) |
| Bitcoin       | Bitcoin addresses  | 1292 (daily, 2012–2016)   |
| PGP WoT       | PGP certificates   | 1500 (daily, 2003–2007)   |
| IPv6 internet | Autonomous systems | 300 (weekly, 2011–2017)   |
| arXiv         | Authors            | 3977 (daily, 2011–2022)   |

(cf. [26], Sec. X), thereby satisfying a necessary condition for predicting connectivity dynamics in real networks. In contrast, as shown, trajectories obtained from synthetic networks that lack an underlying geometry resemble traditional Brownian motion, and are thus unpredictable. From a theoretical perspective, our findings guide the potential development of dynamical models for the nodes' similarity-popularity motion, akin to Langevin equations in molecular dynamics or Newtonian equations in gravitational mechanics [1,7]. Any such equations for networks, to reflect reality, should give rise to the observed subdiffusive dynamics.

More precisely, for each real network, we consider consecutive snapshots of its topology,  $G_1, G_2, \dots, G_\tau$ , spanning the period shown in Table I. We independently map each snapshot  $G_t, t = 1, \dots, \tau$ , to an underlying hyperbolic space using Mercator [13] and extract for each node  $i$  its popularity and similarity trajectories, i.e., the evolution of its popularity and similarity coordinates,  $\{r_i(t), \theta_i(t)\}, t = 1, \dots, \tau$  ([26], Sec. II). We choose to independently map the snapshots in order to avoid possible artificial biases between node coordinates across embeddings, and apply Procrustean rotations [47] to eliminate global rotations and reflections (see Ref. [26], Sec. III).

We note that for each node  $i$  its coordinates  $r_i(t)$  and  $\theta_i(t)$  are inferred from the observed network topology at time  $t$ ,  $G_t$ , and represent estimates for some underlying or “hidden” true coordinates that determine network connectivity [11]. When  $G_t$  changes, these estimates also change. Furthermore, for each node  $i$  we also consider the trajectory of its expected degree  $\kappa_i(t)$ , which is related to  $r_i(t)$  and provides a more direct view on individual node popularity (see Ref. [26], Sec. II). Figures 1(a), 1(f), and 2(a) show the popularity and similarity trajectories of the Charlotte Douglas International Airport (CLT) in the US air transportation network (see Ref. [26], Sec. IX, for other examples).

We find that the obtained trajectories constitute well-defined time series, exhibiting universal properties. Particularly, their velocities (or increments, i.e., differences between consecutive observations) manifest negative auto-correlations with short-term memory [see Figs. 1(b), 1(c), 2(b), and 2(c) and [26], Sec. V]. Furthermore, the velocities exhibit self-similar scale laws of fractional order, i.e., they are of fractal nature [see Figs. 1(d) and 2(d) that are explained below, and [26], Sec. IX, for more examples].

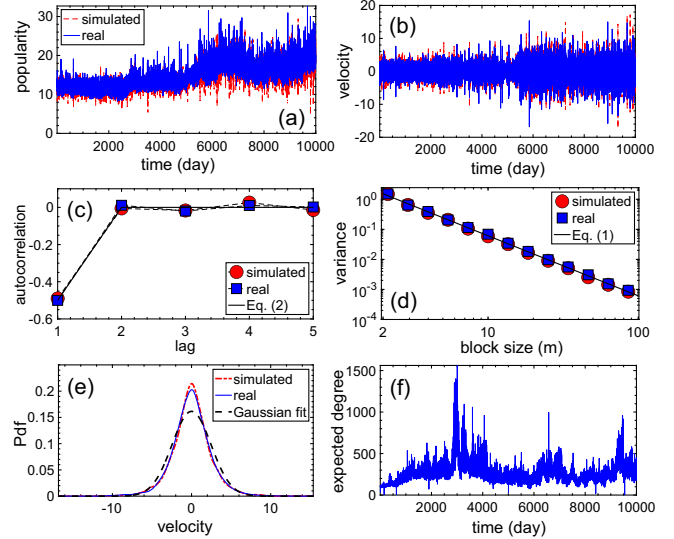


FIG. 1. Properties of the popularity trajectory of CLT in the US air (in blue). (a) Radial popularity trajectory. (b) Trajectory increments (velocity). (c) Sample autocorrelation of the velocity. (d) Variance-time plot of the velocity. (e) Probability density function (PDF) of the velocity. The dashed curve shows a Gaussian PDF with the same mean and variance. (f) Expected degree trajectory. The estimated Hurst exponents for the trajectories in (a) and (f) are 0.0004 and 0.02. The plots show also results for a simulated counterpart of the trajectory (in red) constructed using the model of Eq. (3).

A way to quantify the self-similarity and the type of memory inherited by the trajectories is by computing their Hurst exponent  $H \in (0, 1)$  [48]. A value of  $H$  in  $(0.5, 1)$  indicates a persistent time series with long-range positive

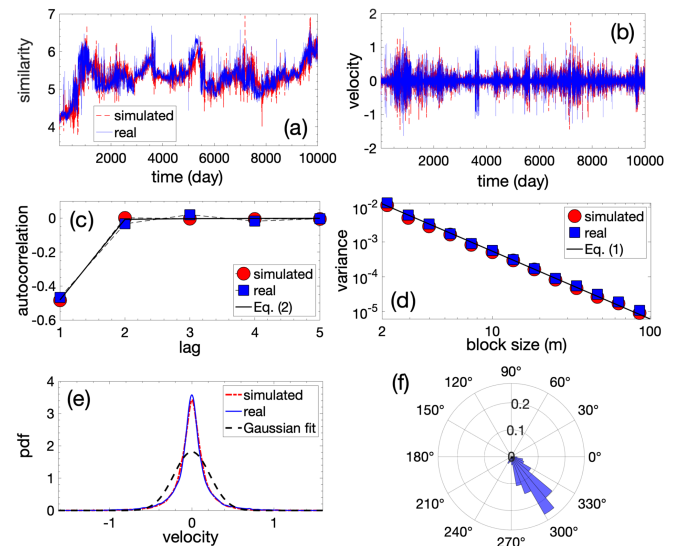


FIG. 2. Properties of the similarity trajectory of CLT in the US air (in blue). (a)–(e) show the same as (a)–(e) in Fig. 1, but for the similarity trajectory. The y axis in (a) is in radians. (f) Angular distribution of the trajectory. The estimated Hurst exponent for the trajectory is 0.03.

autocorrelation (a superdiffusive process). On the other hand, a value of  $H$  in  $(0,0.5)$  indicates an antipersistent or “mean-reverting” time series with negative autocorrelation (a subdiffusive process); in this case, positive (negative) increments tend to be followed by negative (positive) increments, and the dependence between increments is short ranged. The strength of antipersistence increases as  $H$  approaches 0. The case  $H = 0.5$  corresponds to a random process with no dependence between its increments (typical diffusion).

Figure 3 shows the distribution of  $H$  across the trajectories in the US air and IPv6 internet (similar results hold for the other real networks, see Ref. [26], Sec. VI). To calculate  $H$  we use the method of absolute moments [49,50] (see Ref. [26], Sec. IV). We see that, in general, the distributions are concentrated over values of  $H$  well below 0.5, indicating that the trajectories are generally strongly antipersistent. The strongest antipersistence (lowest average  $H$ ) is observed in the US air and Bitcoin, followed by PGP, IPv6, and arXiv (Fig. 3 and [26], Sec. VI). We note that values of  $H$  close to 0 have also been observed in other real data [51,52]. In general, we find that the popularity trajectories are more antipersistent than the similarity trajectories. Figure 3 shows also the distributions of  $H$  in randomized counterparts of the trajectories, obtained by randomizing the sign of the velocities, which breaks correlation ([26], Sec. V). As expected, these distributions are concentrated around  $H = 0.5$ .

To further support our findings, we also construct the variance-time plot [17]. Specifically, let  $X_k^{(m)} = (X_{km-m+1} + \dots + X_{km})/m$ ,  $k = 1, 2, 3, \dots$ , denote an aggregated point series of the velocities over nonoverlapping blocks of size

$m \geq 2$ . Self-similarity implies that the variance of  $X^{(m)}$  satisfies

$$\text{Var}(X^{(m)}) = \sigma^2 m^{2H-2}, \quad (1)$$

where  $\sigma^2$  is the variance of  $X$ . We find that the variance-time plots of the velocity processes, i.e., the empirical plots of  $\log \text{Var}(X^{(m)})$  against  $\log m$ , indeed follow closely Eq. (1) [see Figs. 1(d), and 2(d) and [26], Sec. IX]. We also note that qualitatively similar results hold if we consider network snapshots over coarser time intervals such as weekly or monthly intervals (see Ref. [26], Sec. XI).

To understand the origin of the observed antipersistence, we consider a simple network model where snapshots  $G_t$ ,  $t = 1, 2, \dots, \tau$ , undergo link rewirings (see Ref. [26], Sec. XII). In the geometric version of the model, the snapshots are constructed according to random hyperbolic graphs (RHGs) [10]. Here the nodes are assigned fixed similarity coordinates  $\theta_h$  and target expected degrees  $\kappa_h$ , called “hidden variables,” and are connected with a probability that decreases with their effective distance,  $\Delta\theta_h/(\kappa_h\kappa'_h)$ , where  $\Delta\theta_h$  is the similarity distance and  $\kappa_h, \kappa'_h$  are the nodes’ expected degrees. In the nongeometric version, the snapshots are constructed either according to the configuration model (CM) [53] or to random graphs (RGs) [54]. In CM the connection probability depends only on the nodes’ expected degrees  $\kappa_h, \kappa'_h$ , which are heterogeneous ([26], Sec. XII), while in RGs all nodes have the same expected degree and connected with the same probability. The link-rewiring process involves deleting at random a number of links from snapshot  $G_t$  and subsequently reinserting an equal number of links to generate the next snapshot  $G_{t+1}$ , according to the connection probability in the corresponding model ([26], Sec. XII). Once the snapshots are created, we embed them into hyperbolic spaces and extract the nodes’ expected degree and similarity trajectories,  $\kappa(t)$  and  $\theta(t)$ , following the same procedure as in the real networks.

We find that the trajectories in RHGs exhibit negative autocorrelations and strong antipersistence, as in real networks [see Figs. 4(a) and 4(b) and [26], Figs. S43 and S46]. Further, as in real networks, the similarity trajectories tend to be confined within specific regions of the similarity space [see Figs. 4(c), 4(d), 2(a), and 2(f)]. In contrast, the similarity trajectories in CM and RGs resemble Brownian motion, having Hurst exponents close to 0.5 and spreading throughout the similarity space [see Figs. 4(b), 4(e), and 4(f) and [26], Figs. S44 and S45]. Further, the antipersistence of the degree trajectories weakens [Fig. 4(a) and [26], Figs. S47 and S48].

These results can be explained as follows. In RHGs, even though the snapshots  $G_t$  change, they are all created using the same set of underlying node coordinates. Consequently, the inferred coordinates  $\kappa(t)$  and  $\theta(t)$  for

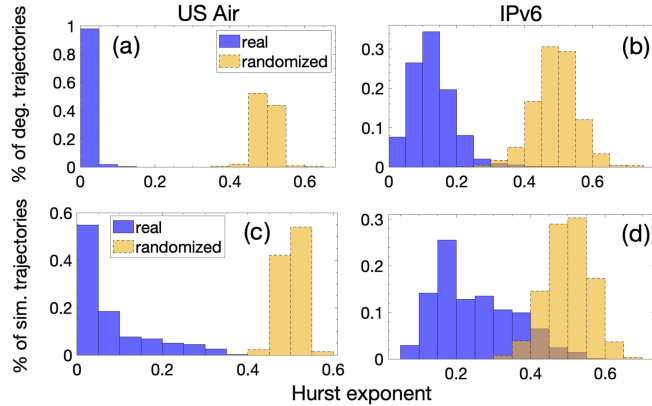


FIG. 3. Distribution of Hurst exponents in US air and IPv6 (in blue). (a) and (b) The expected degree trajectories. The average Hurst exponents are, respectively, 0.01 and 0.13. (c) and (d) The similarity trajectories. The average Hurst exponents are 0.08 and 0.25. We consider trajectories with at least 300 points. The distributions for the randomized counterparts are shown in yellow. Similar results hold for the radial trajectories ([26], Sec. VI).

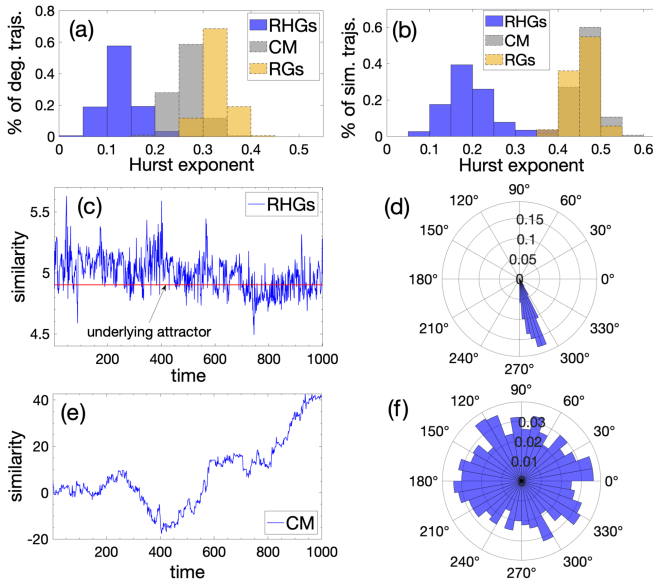


FIG. 4. Expected degree and similarity trajectories in synthetic temporal networks constructed according to RHGs, the CM, and RGs. (a) and (b) The distribution of Hurst exponents for the expected degree and similarity trajectories in the three cases. (c) and (d) A similarity trajectory in RHGs and its distribution in the similarity space. The red line in (c) indicates the underlying attractor, i.e., the node’s hidden similarity coordinate  $\theta_h = 4.9$ . (e) and (f) The same as in (c) and (d), but for the CM case. There is no underlying attractor here. The Hurst exponents for the trajectories in (c) and (e) are, respectively, 0.16 and 0.42.

each node should remain close to their respective underlying coordinates  $\kappa_h$  and  $\theta_h$  at all times  $t$ . Further, whenever the inferred coordinates happen to deviate significantly from their underlying coordinates, then in the subsequent time step it is more likely that they will be closer to them; otherwise, the inferred coordinates would eventually diverge from their underlying coordinates. Additionally, the inferred coordinates never settle onto their underlying ones, which means that whenever they are sufficiently close to them, then in the subsequent time step they are likely to drift away due to probabilistic network changes. In essence, the underlying coordinates of a node can be seen as “attractors” that pull the inferred coordinates close to them. These attractors are in competition with connectivity changes that push the inferred coordinates away from them. This competition explains the observed reversal nature of the trajectories, i.e., antipersistence [Fig. 4(c)].

Nongeometric networks lack underlying similarity attractors, and thus  $\theta(t)$  changes freely, leading to diffusive dynamics [Figs. 4(e) and 4(f)]. Further, although there are still popularity attractors  $\kappa_h$ , degree antipersistence is weaker than in RHGs, as degree trajectories depend on similarity trajectories [13], which are no longer antipersistent. When the attractors  $\kappa_h$  are heterogeneous, tighter constraints are imposed on individual degrees, supporting

the stronger degree antipersistence in CM compared to RGs in Fig. 4(a).

Taken altogether, these results indicate that the observed antipersistence of the real-world trajectories is inherently linked to the latent geometry of real networks, i.e., to their intrinsic similarity-popularity space [12]. We note that the underlying popularity and similarity attractors do not have to remain fixed as in the RHGs model, but can change over time, reflecting long-term popularity and similarity shifts. We also note that subdiffusive and self-similar phenomena, explainable through network geometry, have been previously observed in processes running *on* networks and in the characteristics of network structure, cf. [14]. These phenomena are unrelated to our findings here, which are about the dynamics *of* networks. Next, we show that the trajectories can be well described by a fractional Brownian motion process, and explain how their strong antipersistence favors plausible predictions for their evolution.

Fractional Brownian motion (fBm) indexed by a Hurst exponent  $H$ ,  $B_H(t)$ ,  $t \geq 0$ , is a popular stochastic process often used as basis in the modeling of real-world time series [9]. The increment process of fBm,  $X_H(t) = B_H(t+1) - B_H(t)$ , is called fractional Gaussian noise (fGn) and has the following autocorrelation function [9]:

$$\rho(l) = 0.5(|l+1|^{2H} - 2|l|^{2H} + |l-1|^{2H}), \quad (2)$$

where  $l$  is the time lag.

Figures 1(c) and 2(c) show that Eq. (2) closely follows the empirical autocorrelation function of the velocities. However, Figs. 1(e) and 2(e) show that the velocity distribution is not Gaussian, in contrast to fGn (see Ref. [26], Sec. IX, for other examples). Further, the velocities are characterized by time-varying variances [cf. Figs. 1(b) and 2(b), and [26], Sec. IX]. These facts suggest that standard fBm is rather too simplistic to fully capture the trajectory characteristics. Instead, we find below that an fBm with time-varying noise-induced variance adequately captures the trajectories.

Specifically, we consider a modification of the Riemann-Liouville multifractional Brownian motion model of Ref. [16], where instead of varying the Hurst exponent over time, we vary the noise-induced variance (see Ref. [26], Sec. VII, and Sec. VIII for discussion on multifractality). The model aims to capture trajectories that behave only locally, i.e., within intervals of variance stationarity, as an fBm. Further, we note that trajectories may exhibit both trends and a mean-reverting behavior in their increments. Therefore, we also adjust the model to account for possible trends in the trajectories that can also change with time. The final equation for the considered fBm model takes the form

$$\begin{aligned} \tilde{B}_H(t) = & B_0 + \int_0^t \mu(s) ds \\ & + \frac{1}{\Gamma(H + \frac{1}{2})} \int_0^t (t-s)^{H-1/2} \sigma(s) dB(s), \quad t \geq 0, \end{aligned} \quad (3)$$

where  $B(s)$  is the standard Brownian motion,  $B_0$  is the initial position,  $H \in (0, 1)$  is the Hurst exponent,  $\Gamma$  is the gamma function, and  $\mu(s)$  and  $\sigma(s)$  are, respectively, the trend and noise-induced volatility at time  $s$ . In [26], Sec. VII, we provide the discrete-time analog of the model and explain how to tune its parameters to create simulated counterparts of real trajectories.

Figures 1(a) and 2(a) show that the model can adequately capture the popularity and similarity trajectories of CLT in the US air. In general, we find that the model can capture the trajectories of all the considered networks (see [26], Figs. S10–S34, for other examples), apart from some cases (present mainly in PGP and arXiv) where similarity trajectories appear to exhibit jumps. Such cases suggest that extensions that also account for jumps may be desirable as part of future work [55].

Finally, given the ability of the considered fBm model to simulate trajectories resembling real ones, a natural next question is whether the model can also be used for predicting the future evolution of the trajectories. While a comprehensive assessment of the model's predictive capabilities is beyond the scope of the present work, we provide a glimpse on the model's ability for predictions in [26], Sec. X. We show that predictions are possible, even with simple educated guesses on the model's parameters for the prediction period, based on historical data. This predictability can be explained by the fact that the variance of the considered model grows with time  $t$  as  $t^{2H}$  [9]. Therefore, as real trajectories are typically characterized by low values of  $H \ll 0.5$ , their variance grows slowly with time, remaining even approximately constant for cases where  $H \approx 0$ , favoring their predictability.

Our results pave the way towards the ultimate goal of predicting connectivity dynamics in real networks over different timescales. To accomplish this goal, robust methodologies for trajectory prediction should be developed through automated approaches for fine-tuning the parameters of the proposed model or of possible variations of it. Of particular interest are techniques that can predict changes in the expected trends of the trajectories. In this vein, an interesting direction involves analyzing many trajectories simultaneously, instead of individually, which could identify possible synchronization phenomena across the trajectories and guide the development of dynamical models. Predicting connectivity dynamics would then be equivalent to predicting the evolution of hyperbolic distances among node pairs and deciding on their temporal connectivity based on their distance.

Datasets and code used in the Letter are available at [56].

The authors acknowledge support by the TV-HGGs project (OPPORTUNITY/0916/ERC-CoG/0003), co-funded by the European Regional Development Fund and the Republic of Cyprus through the Research and Innovation Foundation.

\*f.papadopoulos@cut.ac.cy

- [1] D. Krioukov, Brain theory, *Front. Comput. Neurosci.* **8**, 114 (2014).
- [2] DARPA Mathematical Challenges (2007), <https://web.math.utk.edu/~vasili/refs/darpa07.MathChallenges.html>, Accessed: April, 2024.
- [3] D. Easley and J. Kleinberg, *Networks, Crowds, and Markets: Reasoning about a Highly Connected World* (Cambridge University Press, Cambridge, England, 2010).
- [4] A. Gutfraind, Understanding terrorist organizations with a dynamic model, in *Mathematical Methods in Counterterrorism* (Springer Vienna, Vienna, 2009), pp. 107–125.
- [5] B. J. Alder and T. E. Wainwright, Studies in molecular dynamics. I. General method, *J. Chem. Phys.* **31**, 459 (1959).
- [6] S. J. Aarseth, *Gravitational N-Body Simulations: Tools and Algorithms*, Cambridge Monographs on Mathematical Physics (Cambridge University Press, Cambridge, England, 2003).
- [7] T. Schlick, *Molecular Modeling and Simulation: An Interdisciplinary Guide*, Interdisciplinary Applied Mathematics (Springer, New York, 2010).
- [8] R. Friedrich, J. Peinke, M. Sahimi, and M. R. R. Tabar, Approaching complexity by stochastic methods: From biological systems to turbulence, *Phys. Rep.* **506**, 87 (2011).
- [9] B. B. Mandelbrot and J. W. Van Ness, Fractional Brownian motions, fractional noises and applications, *SIAM Rev.* **10**, 422 (1968).
- [10] D. Krioukov, F. Papadopoulos, M. Kitsak, A. Vahdat, and M. Boguñá, Hyperbolic geometry of complex networks, *Phys. Rev. E* **82**, 036106 (2010).
- [11] M. Boguñá, F. Papadopoulos, and D. Krioukov, Sustaining the internet with hyperbolic mapping, *Nat. Commun.* **1**, 62 (2010).
- [12] F. Papadopoulos, M. Kitsak, M. Á. Serrano, M. Boguñá, and D. Krioukov, Popularity versus similarity in growing networks, *Nature (London)* **489**, 537 (2012).
- [13] G. García-Pérez, A. Allard, M. Á. Serrano, and M. Boguñá, Mercator: Uncovering faithful hyperbolic embeddings of complex networks, *New J. Phys.* **21**, 123033 (2019).
- [14] M. Boguñá, I. Bonamassa, M. De Domenico, S. Havlin, D. Krioukov, and M. Serrano, Network geometry, *Nat. Rev. Phys.* **3**, 114 (2021).
- [15] B. B. Mandelbrot, A. J. Fisher, and L. E. Calvet, A multifractal model of asset returns, Cowles Foundation Discussion Paper No. 1164, 1997.
- [16] S. V. Muniandy and S. C. Lim, Modeling of locally self-similar processes using multifractional Brownian motion of Riemann-Liouville type, *Phys. Rev. E* **63**, 046104 (2001).
- [17] W. E. Leland, M. S. Taqqu, W. Willinger, and D. V. Wilson, On the self-similar nature of ethernet traffic, in *Proceedings*

- of ACM SIGCOMM (ACM, New York, USA, 1993), pp. 183–193.
- [18] J. Liu, Y. Shu, L. Zhang, F. Xue, and O. W. W. Yang, Traffic modeling based on FARIMA models, in *Proceedings of the IEEE Canadian Conference on Electrical and Computer Engineering* (1999), Vol. 1, pp. 162–167.
- [19] R. Friedrich and J. Peinke, Description of a turbulent cascade by a Fokker-Planck equation, *Phys. Rev. Lett.* **78**, 863 (1997).
- [20] A. Hadjihosseini, J. Peinke, and N. P. Hoffmann, Stochastic analysis of ocean wave states with and without rogue waves, *New J. Phys.* **16**, 053037 (2014).
- [21] US Department of Transportation—on-time: Reporting carrier on-time performance (1987-present), [https://www.transtats.bts.gov/DL\\_SelectFields.aspx?gnoyr\\_VQ=FGJ&QO\\_fu146\\_anzr=b0-gvzr](https://www.transtats.bts.gov/DL_SelectFields.aspx?gnoyr_VQ=FGJ&QO_fu146_anzr=b0-gvzr), Accessed: July, 2023.
- [22] Kaggle—Bitcoin Dataset for analysis, <https://www.kaggle.com/datasets/chrysanthikosyfaki/bitcoin-dataset-for-analysis>, Accessed: July, 2023.
- [23] OpenPGP Web of Trust Dataset, <https://www.lysator.liu.se/~jc/wotsap/wots2/>, Accessed: July, 2023.
- [24] Ark IPv6 Topology Dataset, [https://www.caida.org/catalog/datasets/ipv6\\_allpref\\_topology\\_dataset/](https://www.caida.org/catalog/datasets/ipv6_allpref_topology_dataset/), Accessed: July, 2023.
- [25] Kaggle—arXiv Dataset, <https://www.kaggle.com/datasets/Cornell-University/arxiv>, Accessed: July, 2023.
- [26] See Supplemental Material at <http://link.aps.org/supplemental/10.1103/PhysRevLett.132.257401> for additional information and discussions, which includes Refs. [27–44].
- [27] OpenPGP, <https://www.openpgp.org/>, Accessed: July, 2023.
- [28] K. Claffy, Y. Hyun, K. Keys, M. Fomenkov, and D. Krioukov, Internet mapping: From art to science, in *Conference For Homeland Security, 2009. CATCH '09. Cybersecurity Applications Technology* (IEEE Computer Society, Los Alamitos, 2009), pp. 205–211.
- [29] A. Muscoloni, J. M. Thomas, S. Ciucci, G. Bianconi, and C. V. Cannistraci, Machine learning meets complex networks via coalescent embedding in the hyperbolic space, *Nat. Commun.* **8**, 1615 (2017).
- [30] F. Papadopoulos, C. Psomas, and D. Krioukov, Network mapping by replaying hyperbolic growth, *IEEE/ACM Trans. Netw.* **23**, 198–211 (2015).
- [31] F. Papadopoulos, R. Aldecoa, and D. Krioukov, Network geometry inference using common neighbors, *Phys. Rev. E* **92**, 022807 (2015).
- [32] Mercator embedding code, <https://github.com/network-geometry/mercator> (2019), Accessed: July, 2023.
- [33] M. S. Taqqu, V. Teverovsky, and W. Willinger, Estimators for long-range dependence: An empirical study, *Fractals* **03**, 785 (1995).
- [34] S. C. Lim, Fractional Brownian motion and multifractional Brownian motion of Riemann-Liouville type, *J. Phys. A* **34**, 1301 (2001).
- [35] S. Rambaldi and O. Pinazza, An accurate fractional Brownian motion generator, *Physica A (Amsterdam)* **208**, 21 (1994).
- [36] giannit, Fractional and Multifractional Brownian motion generator, <https://github.com/Rabelaiss/mBm> (2022), Accessed: July, 2023.
- [37] S. Bianchi, Pathwise identification of the memory function of multifractional Brownian motion with application to finance, *Int. J. Theor. Appl. Finance* **8**, 255 (2005).
- [38] H. Wendt and P. Abry, Multifractality tests using bootstrapped wavelet leaders, *IEEE Trans. Sig. Process.* **55**, 4811 (2007).
- [39] S. Jaffard, B. Lashermes, and P. Abry, Wavelet leaders in multifractal analysis, in *Wavelet Analysis and Applications* (Birkhäuser Basel, Basel, 2007), pp. 201–246.
- [40] A.-L. Barabási and T. Vicsek, Multifractality of self-affine fractals, *Phys. Rev. A* **44**, 2730 (1991).
- [41] Z.-Q. Jiang, W.-J. Xie, W.-X. Zhou, and D. Sornette, Multifractal analysis of financial markets: A review, *Rep. Prog. Phys.* **82**, 125901 (2019).
- [42] A. Y. Schumann and J. W. Kantelhardt, Multifractal moving average analysis and test of multifractal model with tuned correlations, *Physica A (Amsterdam)* **390**, 2637 (2011).
- [43] J. Ludescher, M. I. Bogachev, J. W. Kantelhardt, A. Y. Schumann, and A. Bunde, On spurious and corrupted multifractality: The effects of additive noise, short-term memory and periodic trends, *Physica A (Amsterdam)* **390**, 2480 (2011).
- [44] J. Park and M. E. J. Newman, Statistical mechanics of networks, *Phys. Rev. E* **70**, 066117 (2004).
- [45] S. N. Dorogovtsev, *Lectures on Complex Networks* (Oxford University Press, Oxford, 2010).
- [46] M. J. Saxton, A biological interpretation of transient anomalous subdiffusion, I. Qualitative model. *Biophys. J.* **92**, 1178 (2007).
- [47] F. J. Rohlf and D. Slice, Extensions of the procrustes method for the optimal superimposition of landmarks, *Syst. Biol.* **39**, 40 (1990).
- [48] H. E. Hurst, Long-term storage capacity of reservoirs, *Trans. Am. Soc. Civil Eng.* **116**, 770 (1951).
- [49] T. Preis, P. Virnau, W. Paul, and J. J. Schneider, Accelerated fluctuation analysis by graphic cards and complex pattern formation in financial markets\*, *New J. Phys.* **11**, 093024 (2009).
- [50] A. Z. Górski, S. Drożdż, and J. Speth, Financial multifractality and its subtleties: An example of DAX, *Physica A (Amsterdam)* **316**, 496 (2002).
- [51] J. Gatheral, T. Jaisson, and M. Rosenbaum, Volatility is rough, *Quant. Finance* **18**, 933 (2018).
- [52] E. Neuman and M. Rosenbaum, Fractional Brownian motion with zero Hurst parameter: A rough volatility viewpoint, *Electron. Commun. Probab.* **23**, 1 (2018).
- [53] F. Chung and L. Lu, The average distances in random graphs with given expected degrees, *Proc. Natl. Acad. Sci. U.S.A.* **99**, 15879 (2002).
- [54] R. Solomonoff and A. Rapoport, Connectivity of random nets, *Bull. Math. Biophys.* **13**, 107 (1951).
- [55] W.-L. Xiao, W.-G. Zhang, X.-L. Zhang, and Y.-L. Wang, Pricing currency options in a fractional Brownian motion with jumps, *Econ. Model.* **27**, 935 (2010).
- [56] E. S. Papaefthymiou, C. Iordanou, and F. Papadopoulos, Fundamental dynamics of popularity-similarity trajectories in real networks repository, <https://github.com/cosior/TV-HGG> (2024).